PHYSICAL REVIEW B **85**, 195324 (2012)

Excitation of spin waves in ferromagnetic (Ga,Mn)As layers by picosecond strain pulses

M. Bombeck,[1] A. S. Salasyuk,[1,2] B. A. Glavin,[3] A. V. Scherbakov,[2] C. Brüggemann,[1] D. R. Yakovlev,[1,2] V. F. Sapega,[2] X. Liu,[4] J. K. Furdyna,[4] A. V. Akimov,[2,5] and M. Bayer[1,2]

[1]*Experimentelle Physik 2, Technische Universität Dortmund, D-44227 Dortmund, Germany*

[2]*Ioffe Physical-Technical Institute, Russian Academy of Sciences, 194021 St. Petersburg, Russia*

[3]*Department of Theoretical Physics, V.E. Lashkaryov Institute of Semiconductor Physics, 03028 Kyiv, Ukraine*

[4]*Department of Physics, University of Notre Dame, Notre Dame, Indiana 46556, USA*

[5]*School of Physics and Astronomy, University of Nottingham, Nottingham NG7 2RD, United Kingdom*

(Received 25 October 2011; revised manuscript received 18 January 2012; published 25 May 2012)

We report the excitation of spin waves in ferromagnetic semiconductor (Ga,Mn)As films by picosecond strain pulses. The strain pulse with a broad acoustic spectrum excites a number of magnon modes, which contribute to the precession of magnetization. The spectrum of the excited spin waves shows two well-resolved peaks with intensities dependent on the applied magnetic field. For a certain range of magnetic fields only the low-frequency spin wave is detected. We present the theoretical analysis and compare it with the experimental results, addressing the spatial overlap of the magnon and phonon eigenfunctions. Depending on the boundary conditions and the spectrum of the spin waves the spatial matching of the spin wave and resonance phonon eigenfunctions may provide high excitation efficiency for only one magnon mode, while other modes are not excited.

DOI: 10.1103/PhysRevB.85.195324 PACS number(s): 76.50.+g, 75.50.Pp, 75.78.Jp, 78.20.hc

I. INTRODUCTION

The enormous success of semiconductors is based on the possibility to tailor their electrical and optical properties almost arbitrarily. This has stimulated activities to seek such a level of control also for their magnetic properties which might allow all-in-one-chip solutions in information technology. Ferromagnetic semiconductors, on whose basis ultrafast magnetoelectronic and magneto-optical devices[1] may become operational, are a key building block on this route. While great progress has already been achieved in this area, considerable obstacles still need to be overcome. This concerns not only the development of highest quality material, but also novel tools, distinctly different from established ones, for manipulating and controlling the magnetization may be required.

An example of such a novel concept is the recent demonstration that the interaction between spin waves (SWs) may be used for spin current control.[2] During the last decade, the underlying magnon excitations with frequencies in the gigahertz range have been intensively studied experimentally and theoretically for ferromagnetic (Ga,Mn)As.[3–8] These activities were focused on thin ferromagnetic films in which SWs have a discrete frequency spectrum determined by parameters such as magnetocrystalline anisotropy, spin exchange interaction, layer thickness and boundary conditions. For SW applications, it is essential to control the amplitude of various SW modes. In particular, it is attractive to have a technique that allows selective excitation of a single SW mode with particular frequency/wavelength while all other modes have zero amplitude. The most common technique to achieve this is microwave excitation at a frequency resonant with the SW mode.[2–4,6–8] While nicely functioning, microwave manipulation is limited to nanosecond time scales and cannot be scaled down to submicrometer spatial dimensions. Optical excitation of SWs has also been demonstrated, but this excitation does not show a dependence of the SW amplitudes on magnetic field and thus it is not frequency selective.[5]

In this paper, we demonstrate an approach to excite SW modes in a ferromagnetic layer using picosecond strain pulses with a broad acoustic phonon spectrum that overlaps the SW frequencies. Using this picosecond acoustic technique, which is a well developed method by now, we excite various SW modes and find that their relative amplitudes depend on the applied magnetic field. We analyze the excitation of SWs theoretically and attribute the experimental observation to the spatial overlap of the SW mode and the resonant component in the phonon spectrum. A theoretical picture reveals the strong sensitivity of this type of excitation to magnetic boundary conditions and SW frequency. The goal of the present work is to show that despite of all complications reliable conditions for single SW mode excitation can be obtained in the experiment.

II. EXPERIMENT

The studied sample is a single $Ga_{0.95}Mn_{0.05}As$ layer with thickness $d = 200$ nm grown by low-temperature molecular-beam epitaxy on top of a semi-insulating (001) GaAs substrate. The Curie temperature of the ferromagnetic layer is 60 K and the saturation magnetization is 20 emu/cm^3. The layer is compressively strained normal to the growth direction leading to an in-plane orientation of the easy axis of magnetization.

Figure 1(a) shows the schematic of the experiment, which was carried out at temperature $T = 6$ K in a cryostat with a superconducting magnet. The external magnetic field **B** is applied in the layer plane parallel to the easy axis, denoted as x axis. For picosecond strain pulse generation,[9] optical pulses from a femtosecond laser (wavelength 800 nm, pulse duration 150 fs, pulse energy density 2 mJ/cm^2, repetition rate 100 kHz) excite a 100-nm thick Al film deposited on the back side of the GaAs substrate. The strain pulse injected into the GaAs substrate has a duration of $\sim$20 ps with a maximum amplitude $\sim 1 \times 10^{-4}$. Figures 1(b) and 1(c) show the time dependence and the corresponding frequency spectrum of the injected strain pulse $\varepsilon_{in}(t)$ respectively. The pulse propagates

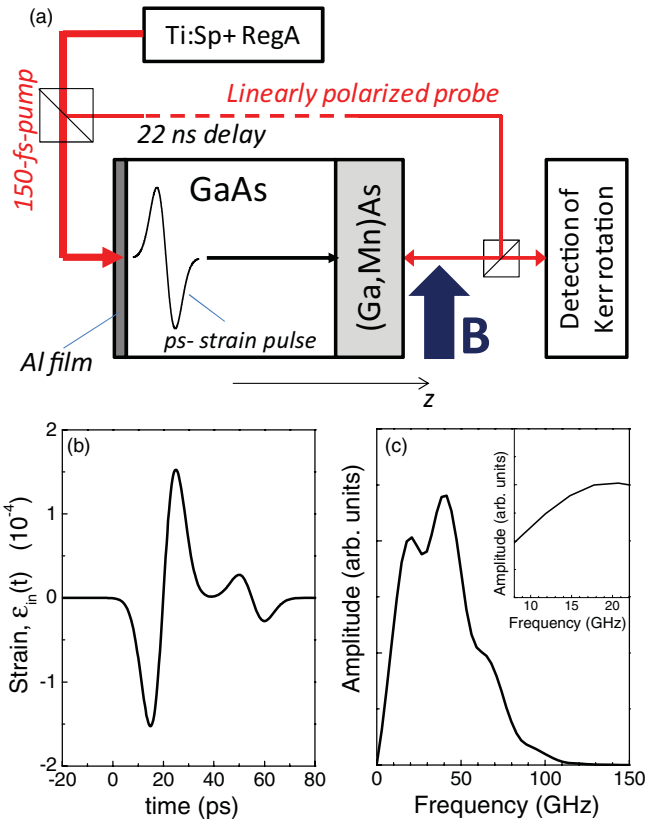

FIG. 1. (Color online) (a) The schematic of experiment with picosecond strain pulses. (b) Time profile of the strain pulse, $\varepsilon_{\text{in}}(t)$, injected into the GaAs substrate. (c) Fourier spectrum of the strain pulse; the inset shows the spectral part corresponding to the range of magnetization precession frequencies experimentally observed.

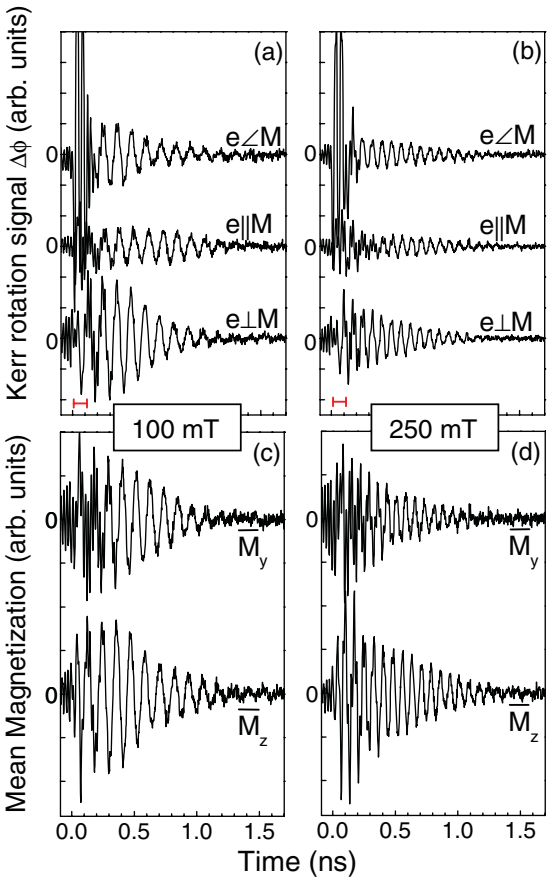

FIG. 2. (Color online) (a) and (b) Kerr rotation signals measured for various polarizations of the probe beam at applied magnetic fields of $B = 100$ mT (a) and 250 mT (b); the horizontal bars indicate the time intervals during which the strain pulse is present inside the film. (c) and (d) Temporal evolutions of the mean magnetization projections $\overline{M}_z(t)$ and $\overline{M}_y(t)$ for the same B as in (a) and (b), obtained from the measured Kerr rotation signals using Eq. (1).

normal to the layer through the GaAs substrate (along the z axis) at longitudinal sound velocity $s = 4.8$ km/s, and after $t_0 = l_0/s \approx 22$ ns reaches the (Ga,Mn)As magnetic layer ($l_0 = 105$ μm is the GaAs substrate thickness). There it passes through the layer, becomes reflected at the open sample surface with a π-phase shift, and travels back towards the GaAs substrate. At $T = 6$ K for the initial strain amplitude of $\sim 10^{-4}$, scattering as well as nonlinear effects are insignificant[10] and we may assume that the strain pulse propagates in the sample keeping its initial shape and spectral content.

While propagating through the (Ga,Mn)As layer, the strain pulse modifies the magneto-crystalline anisotropy at each spatial (z) position as a function of time (t), causing the magnetization $\mathbf{M}$ to be turned out of the equilibrium orientation, which is approximately parallel to the [100] axis. The magnitude of this turn and the corresponding tilt angle were discussed in earlier works.[11,12] After the strain pulse has left the magnetic film, the subsequent dynamics of $\mathbf{M}(z,t)$ shows harmonic oscillations of the M_z and M_y components.

The effect on the magnetization dynamics induced by the strain pulse is measured by monitoring the Kerr rotation angle $\phi(t)$ as function of the delay of a probe laser pulse relative to the pump pulse, both taken from the same laser. The pump beam is modulated by a mechanical chopper, and $\Delta\phi(t) = \phi(t) - \phi_0$ is recorded (ϕ_0 being the Kerr rotation angle without strain pulses). Examples of the signals $\Delta\phi(t)$ measured at $B = 100$ and 250 mT for three different polarization settings of the probe beam are shown in Figs. 2(a) and 2(b). Different temporal regimes are seen for the oscillatory behavior of $\Delta\phi(t)$. The high-frequency features in the interval $t < 0.1$ ns result mainly from elastooptical effects, as described in detail in the recent work by Thevenard *et al.*[13] For times $t > 0.1$ ns, i.e., after the strain pulse has left the (Ga,Mn)As layer, the oscillations correspond exclusively to magnetization precession. In the experimentally used geometry for which the direction of $\mathbf{M}_0$ is close to the [100] axis, the evolution of $\Delta\phi(t)$ depends on the angle between the probe polarization plane and the [100] direction, ψ, and may be written as

$$\Delta\phi(t) = a\overline{M}_z(t) + b\overline{M}_y(t)\cos 2\psi + c(t)\sin 2\psi. \qquad (1)$$

The first two terms in Eq. (1) give the dynamics of the layer magnetization, which in general evolve spatially nonuniform. Here, a and b are constants and $\overline{M}_{z,y}(t)$ are determined by the spatial distributions of the magnetization and the probe light field inside the magnetic layer. In case of no light absorption and no reflection at the (Ga,Mn)As/GaAs interface, we have $\overline{M}_z(t) = \frac{1}{d}\int_0^d M_z(z,t)\cos[2k_{\text{ph}}(z-d)]dz$ and $\overline{M}_y(t) = \frac{1}{d}\int_0^d M_y(z,t)\sin[2k_{\text{ph}}(z-d)]dz$, where the magnetic layer is

located at $0 < z < d$ and k_{ph} is the photon wave number in the layer. The contributions of the z and y magnetization components to the rotation of probe polarization are due to the magnetooptical anisotropy and are governed by the circular[14] and giant linear[15] dichroism in (Ga,Mn)As, respectively. The third term in Eq. (1) describes the dynamical photoelastic perturbation induced by the strain pulse in the presence of a static magnetooptical anisotropy of the magnetic layer.[13] The constants a, b, and the dependence $c(t)$ are not known with high precision. Nevertheless, Eq. (1) allows us to extract $\overline{M}_z(t)$ and $\overline{M}_y(t)$ from measurements of $\Delta\phi(t)$ for three different probe beam polarizations $\mathbf{e}$: e.g., for $\mathbf{e}\|\mathbf{M_0}$, $\mathbf{e}\perp\mathbf{M_0}$, and $e\angle M_0$ with an angle of 45° between $\mathbf{e}$ and $\mathbf{M_0}$. The resulting evolutions of $\overline{M}_z(t)$ and $\overline{M}_y(t)$ for the two B values from above are shown in Figs. 2(c) and 2(d). Figure 3(a) shows fast Fourier transform spectra of $\overline{M}_z(t)$ for different B. The spectra obtained from $\overline{M}_y(t)$ look similar. Generally, two spectral lines are seen whose central frequencies, f_l and f_h, shift smoothly to higher values with increasing B, while the spacing $\Delta f = f_h - f_l \approx 2$ GHz between them remains almost constant, see Fig. 3(b). The solid line in Fig. 3(b) shows the calculated magnetic field dependence[16] of the spatially uniform magnetization precession frequency, which correlates well with that of f_l, supporting the origin of the observed signal in the magnetization precession. The amplitudes of the two spectral lines vary with magnetic field. The most interesting feature in this respect is that at fields around $B = B_0 = 225 \pm 25$ mT, only a single line corresponding to the lower frequency component is observed. This is also demonstrated by Fig. 3(c), which shows the peak intensities of the low- and high-frequency spectral lines versus B. Both vary nonmonotonically with B, and the high-frequency spectral line disappears around $B = B_0$, while the low frequency one is still present. The dependence of the spectrum on magnetic field is the main experimental observation of the present work. Earlier work[5] in which SWs were excited optically, also demonstrated a doublet of lines in the SW spectrum, but the amplitudes of the peaks did not depend on B. Thus the present tool using picosecond strain pulses may represent an exceptional instrument for controlled SW excitation.

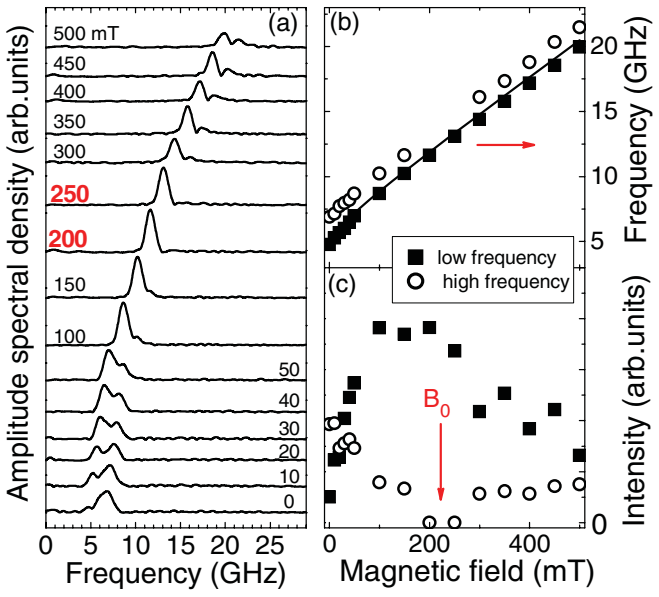

FIG. 3. (Color online) (a) Amplitude spectra, obtained by FFT of the temporal curves in a 2-ns time window for the z projection of the magnetization at different applied magnetic fields, indicated at each curve. The B values for which only low frequency SW mode is detected are highlighted. (b) Central frequencies of the excited SW modes as functions of B. The solid line shows the calculated frequency of the spatially uniform magnetization precession. The magnetic anisotropy parameters were chosen close to those derived for a similar sample (see Ref. 16). (c) Magnetic field dependencies of the peak intensities of the low- and high-frequency SW modes. The arrows in (b) and (c) indicate the frequency and magnetic field around which single spectral line is observed.

III. THEORETICAL ANALYSIS AND DISCUSSION

The physics underlying SW excitation is related to the spin-phonon interaction in ferromagnetic materials, as discussed in literature.[17] In bulk materials, energy and momentum conservation for the spin-phonon interaction result in strict selection rules for the SW excitation or, in case of strong coupling, for excitation of hybrid magnon-phonon modes. In thin films, momentum conservation is relaxed so that a monochromatic acoustic wave may excite a resonant standing SW independent of its wavelength.[18] In our experiments, the ultrashort strain pulse corresponds to an acoustic phonon wave packet that contains a broad distribution of frequencies, so that the excitation cannot be considered as monochromatic. Nevertheless, we show below that a strain pulse, propagating through the layer in forward and, subsequently, in backward direction, excites SW modes whose amplitudes are strongly dependent on the SW frequency and thus on B. Moreover, for certain conditions, only a single SW mode may be excited by the strain pulse. For this purpose, we analyze the magnetization dynamics by the Landau-Lifshitz equation[19]:

$$\frac{\partial \mathbf{M}}{\partial t} = -\gamma \mathbf{M} \times \left(-\nabla_{\mathbf{M}} F + \frac{D}{M_0} \nabla^2 \mathbf{M} \right), \qquad (2)$$

where γ, F, D, and M_0, are the gyromagnetic ratio, the magnetic free energy density, the exchange stiffness constant, and the magnetization magnitude, respectively. F contains contributions determined by the magnetic layer properties and the applied magnetic field. In addition to the case of an unstrained crystal, F contains also magnetoelastic terms for biaxially strained (Ga,Mn)As.[20]

The strain pulse propagation through the magnetic layer causes a variation of F in time, t, and space, z, resulting in a complicated trajectory of **M.** When the strain pulse leaves the magnetic layer, $\mathbf{M}$ continues to precess about its equilibrium position while relaxing towards $\mathbf{M_0}$ [note that relaxation is not included in Eq. (2)]. During this precession, the asymptotic solutions of the magnetization components M_i can be obtained in linear approximation in which the deviation from steady-state $\delta\mathbf{M}(z,t) = \mathbf{M}(z,t) - \mathbf{M}_0$ is written as a superposition of standing SW eigenmodes $S_i^{(n)}(z)$:

$$\delta M_i(z,t) = \sum_{n=0}^{\infty} C^{(n)} S_i^{(n)}(z) \cos\left(\omega_n t + \alpha_i^{(n)}\right), \qquad (3)$$

where the $C^{(n)}$ and $\alpha_i^{(n)}$ are the stationary amplitude and phase of the nth mode with frequency ω_n ($n = 0, 1, 2, \ldots$). Calculation of the mode amplitudes $C^{(n)}$ shows that they are proportional to the overlap integrals:

$$C^{(n)} \sim \int_0^d \varepsilon^{(n)}(z) S_i^{(n)}(z) dz, \tag{4}$$

where $\varepsilon^{(n)}(z)$ is the spatial distribution of the strain pulse Fourier component with phonon frequency identical to that of the SW, ω_n, in the magnetic layer (see Appendix).

In order to evaluate the overlap integral Eq. (4), we need to know $\varepsilon^{(n)}(z)$ and $S_i^{(n)}(z)$. The properties of the propagating spatial strain pulse were studied in numerous works experimentally and theoretically using various approaches (see, for example, Refs. 21 and 22). It is known that the shape of the strain pulse injected into the substrate is similar to that shown in Fig. 1(b). For strain amplitudes $\leqslant 10^{-4}$ and low temperatures ($T < 100$ K), the damping is not essential and the spatial profile of the initial strain pulse is approximately conserved while travelling through the substrate. Thus, at any coordinate, the time evolution of the strain induced by the initial strain pulse $\varepsilon_{\text{in}}(t)$ traveling toward the open surface of the sample is $\varepsilon(z,t) = \varepsilon_{\text{in}}(t - z/s)$. In the frequency range between 8 and 20 GHz, relevant for our case, the Fourier spectrum of the strain pulse is a smooth function of frequency [see the inset in Fig. 1(c)]. It is important that the z dependence of the strain harmonics $\varepsilon^{(n)}(z)$ is governed by the properties of the acoustic wave reflection from the free surface at $z = d$, namely, by the requirement of zero stress at surface of the sample. Neglecting nonlinearity and dispersion during pulse propagation through the magnetic film, we can express the strain as a superposition of the incident and the reflected components: $\varepsilon(z,t) = \varepsilon_{\text{in}}(t - z/s) - \varepsilon_{\text{in}}[t + (z - 2d)/s]$. Accordingly, we get

$$\varepsilon^{(n)}(z) = 2i \exp(i\omega_n d/s)\varepsilon_{\text{in}}^{(\omega_n)} \sin[\omega_n(z - d)/s], \tag{5}$$

where $\varepsilon_{\text{in}}^{(\omega_n)}$is the spectral amplitude of the initial strain pulse at frequency ω_n. The z-dependent factor $\sin[\omega_n(z - d)/s]$ is the key feature which, as we will see below, determines the efficiency of excitation of a certain SW mode. This factor is independent of the particular shape of the strain pulse, which enters the expression for $\varepsilon^{(n)}(z)$ only through the spectral amplitude.

A. The role of magnetic boundary conditions

The SW eigenmodes $S_i^{(n)}(z)$ and their frequency spectrum depend on the magnetic boundary conditions. These conditions have major impact on the analysis of the SW amplitudes governed by the overlap integral in Eq. (4). In this section, we present the results of model calculations of SW amplitudes for various boundary conditions. The aim of this consideration is to show that the SW amplitudes are strongly dependent on the magnetic field due to the dependence of the overlap integral Eq. (4) on the resonance frequency, and for certain conditions only one SW mode may be excited.

Within the macroscopic Landau-Lifshitz approach, the boundary conditions can be introduced through the surface magnetic energy F_{surf}. Most commonly, it is assumed that $F_{\text{surf}} = K_s \cos^2\theta$ (where θ is the angle between $\mathbf{M}$ at the surface and the normal to the surface $\mathbf{n}$). The surface magnetic energy parameter K_s depends on the surface easy axis, that can be oriented either normal ($K_s < 0$) or parallel to the surface ($K_s > 0$). Then the boundary conditions can be written as $\mathbf{M} \times (D\frac{\partial \mathbf{M}}{\partial \mathbf{n}} + 2\mathbf{n}K_s \cos\theta) = 0$.[23]

For (Ga,Mn)As, the magnetic boundary condition parameters have been discussed intensively during the last decade but the problem is still unsolved.[3–8] Three extreme cases were reported earlier for (GaMn)As with $\mathbf{M}_0$ close to [100]:[5,6] (i) extremely high values of $K_s > 0$, almost equivalent to the pinning boundary conditions $M_{z,y} = 0$; (ii) $K_s = 0$, which corresponds to a "free surface" with $\frac{\partial M_{x,y}}{\partial z} = 0$; and (iii) $K_s < 0$, where typically surface- and bulklike modes exist in the SW spectrum.

First, we analyze the amplitudes of the SWs assuming the pinning conditions at the interfaces ($K_s > 0$). For homogeneous magnetic properties of the film, one easily obtains $S_i^{(n)} \sim \sin[\pi(n + 1)z/d]$ (see Ref. 24) and from Eqs. (4) and (5) for the amplitude of nth SW mode we can write

$$C^{(n)} \sim \frac{(n + 1)\sin \pi x_n}{x_n^2 - (n + 1)^2}, \tag{6}$$

where $x_n = \omega_n d/(\pi s)$.

For simplicity, we consider the frequency spacing between different modes to be much less than the fundamental frequency ω_0. Then the $\varepsilon^{(n)}(z)$ are almost the same for all SW eigenmodes and we may assume $\varepsilon^{(n)}(z) = \varepsilon^{(0)}(z)$ for any mode number, n. The results of calculation for this simplified case are presented in Fig. 4. The solid lines in Fig. 4(a) show the

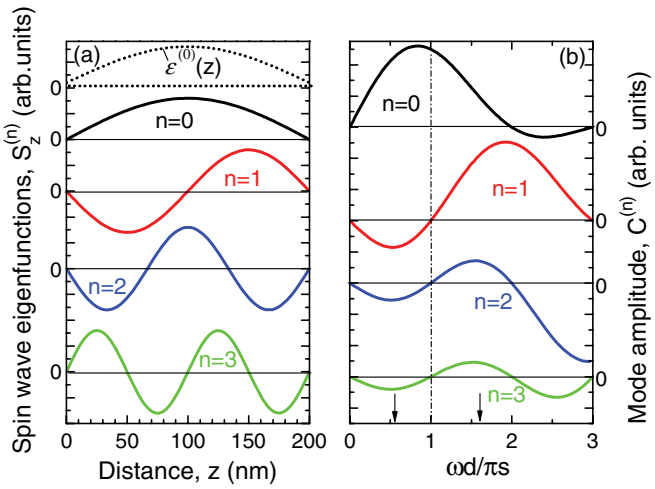

FIG. 4. (Color online) (a) Spin wave eigenfunctions (solid lines) of the four lowest modes calculated for pinning boundary conditions ($K_s > 0$). The dotted line shows the spatial dependence of the Fourier component of the acoustic wave packet in the strain pulse with frequency ω_0, which corresponds to the condition $\omega_0 d/\pi s = 1$ and is equal to 12 GHz for the studied structure. (b) Dependencies of the SW mode amplitude on the normalized resonance frequency $\omega d/\pi s$ for the four lowest modes. The vertical dash-dotted line corresponds to the frequency at which only the ground mode $n = 0$ is excited. The vertical arrows indicate the frequencies related to the experimental conditions at $B = 0$ and $B = 500$ mT.

spatial shapes of $S_z^{(n)}(z)$ for the four lowest modes ($n = 0$, 1, 2, and 3). The amplitudes $C^{(n)}$ of these modes as functions of the dimensionless parameter $\omega d/\pi s$ are shown in Fig. 4(b). We see that all the SW modes have an oscillating shape with the number of oscillations increasing with the increase of n. In general, they all can be excited by the strain pulse in the whole range of frequencies. The relative amplitudes of the excited SW mode depend on the frequency and correspondingly on the applied magnetic field, which determines ω_n, but for certain values of ω only a single SW mode has nonzero amplitude. From Eq. (7) we obtain that if the parameter $\omega d/\pi s$takes on an integer value, i.e.,

$$\frac{\omega d}{\pi s} = (n+1) \quad \text{and} \quad n = 0,1,2,\ldots, \tag{7}$$

only the nth SW mode is excited, while the amplitude of all other modes is equal to zero. The lowest fundamental mode ($n = 0$) may be the only excited mode if $\omega_0 d/\pi s = 1$ [indicated by the vertical dashed line in Fig. 4(b)]. The dashed line in Fig. 4(a) shows the spatial distribution of the corresponding resonant harmonic of the strain pulse $\varepsilon^{(0)}(z) \sim \sin[\omega_0(z-d)/s]$, which has two nodes at the interfaces of the magnetic layer. Obviously, the overlap integral of $\varepsilon^{(0)}(z)$ with $S_z^{(n)}(z)$ is nonzero only for the fundamental mode $S_z^{(0)}$.

Figures 5 and 6 show the results of calculations performed for the other boundary conditions, assuming either a free surface ($K_s = 0$) or mixed bulk- and surface-like modes ($K_s < 0$). In these cases, the amplitudes $C^{(n)}$ also depend strongly on SW mode number n and frequency ω, but the exact dependencies are very different from those for pinning boundary conditions. In particular, $C^{(n)} = 0$ for some values of n and ω, but the calculations do not show the excitation of a single SW at any ω.

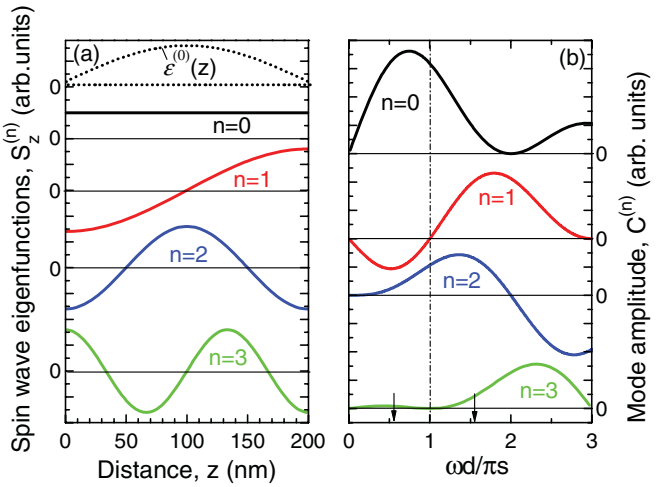

FIG. 5. (Color online) (a) Spin wave eigenfunctions (solid lines) of the four lowest modes calculated for "free-surface" boundary conditions ($K_s = 0$). The dotted line shows the spatial dependence of the Fourier component of the strain pulse with frequency $\omega_0 = 12$ GHz. (b) Dependencies of the SW mode amplitude on the normalized resonance frequency $\omega d/\pi s$ for the four lowest modes. The vertical dash-dotted line corresponds to the frequency $\omega = 12$ GHz at which $\omega d/\pi s = 1$. The vertical arrows indicate the frequencies related to the experimental conditions at $B = 0$ and $B = 500$ mT.

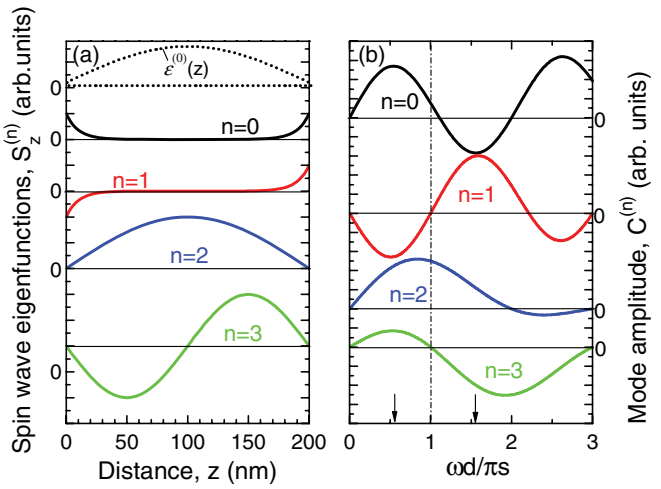

FIG. 6. (Color online) (a) Spin wave eigenfunctions (solid lines) of the four lowest modes calculated for the boundary conditions, which give mixed surface- and bulk-like modes in the SW spectrum ($K_s < 0$). The dotted line shows the spatial dependence of the Fourier component of the strain pulse with frequency $\omega_0 = 12$ GHz. (b) Dependencies of the SW mode amplitude on the normalized resonance frequency $\omega d/\pi s$ for the four lowest modes. The vertical dash-dotted line corresponds to the frequency $\omega = 12$ GHz at which $\omega d/\pi s = 1$. The vertical arrows indicate the frequencies related to the experimental conditions at $B = 0$ and $B = 500$ mT.

B. Comparison with experiment

The model calculations clearly show that the amplitudes of various SW modes excited by the strain pulse depend on magnetic field and this dependence is governed by the magnetic boundary conditions. The boundary conditions for (Ga,Mn)As are debated widely in literature, but, unfortunately, it is impossible to assess what boundary conditions should be applied in our particular experimental case.

Comparing the experimental data and the theoretical results we need to choose boundary conditions so, that the two lowest SW modes have a frequency separation equal to $\Delta f = f_h - f_l = 2$ GHz and only the lowest SW mode is excited at $B = 225$ mT. Indeed, for the case $K_s < 0$, we can find values of D and K_s ($D = 5 \times 10^{-18}$ Tm^2 and $2K_s/D = -1.2 \times 10^{-9}$ Tm), which give the frequency separation between the lowest surface-like and bulklike modes of about 2 GHz and this value is almost independent on B. However, the calculated field dependence of excitation efficiency given by Eq. (4) (see Fig. 6) does not demonstrate a single spectral line around 12 GHz in the field range B = 200 ÷ 250 mT that is measured experimentally. Alternatively, for large positive K_s corresponding to the pinning boundary conditions, we get perfect agreement between the calculated and experimental field dependencies of the SW modes amplitudes. Indeed, the single line observed in the measured spectrum around $B = B_0$ [see Fig. 3(a)] has the frequency $f_l = 12$ GHz, corresponding to the fundamental radial frequency ω_0 given by Eq. (7). Thus, for the assumed magnetic pinning boundary conditions, we

have excellent agreement with the experiment if we associate the lower frequency (f_l) spectral line with the fundamental SW mode ($n = 0$). However, it is not possible to find a reasonable value of D, which would provide 2 GHz frequency splitting between the lowest SW modes.[6] Thus we cannot unambiguously attribute the high-frequency (f_h) spectral line observed in the experiment with the SW mode with $n = 1$. Additional ambiguity in the theoretical analysis of the signal spectra comes from the fact that the probe wavelength is close to the fundamental absorption band, and we cannot analyze quantitatively the efficiency of optical detection for various SW modes.

Apparently, the problems in getting agreement for both the spectrum and amplitude for various SW modes could be solved for a wider class of boundary conditions. This should happen as long as the mode's spatial structure is determined by volume inhomogeneities of the magnetic anisotropy parameters, suppressing the magnitude of magnetization near the interfaces.[6] Although it is difficult to assess the mode amplitudes for this case quantitatively, the fast spatial oscillations of the eigenfunctions $S_z^{(n)}(z)$ with $n > 0$ suggest that the efficiency of their excitation is small, if the condition (7) is fulfilled for the mode with $n = 0$.

The consideration given in the theory section does not include the dissipation of SW modes. In principle, one cannot completely exclude resonance conditions for interaction of SWs with other excitations (e.g., plasmons, incoherent phonons), which could result in strong damping of the upper SW mode at $B = B_0$. This statement however is too speculative and we do not consider details in the present paper.

IV. CONCLUSION

We have demonstrated the excitation of spin wave modes in a (Ga,Mn)As layer by picosecond strain pulse. We find a strong dependence of the amplitudes of the excited SWs on the magnetic field and, consequently, on the SW frequency. Only one spectral line, which can be attributed to the fundamental SW mode, is observed when the magnetization precession period is equal to the strain pulse travel time forward and backward through the magnetic layer. This observation is discussed and analyzed theoretically in terms of excitation efficiency, which depends crucially on the spatial shape of magnetization of distinct SW modes and their overlap with the corresponding Fourier component in the acoustic wave packet. In spite of difficulties in getting full agreement between theory and experiment for SW frequencies and amplitudes, we show that it is possible to realize the case when only one SW mode is excited. Such selective excitation of one SW mode opens potential in various applications.

The technique of exciting SWs by picosecond strain pulses is a prospective tool for spin current manipulation in devices in which hypersonic nanostructures, like phonon cavities[25] or sasers,[26,27] are combined with electromagnetic and optomagnetic components in a single semiconductor chip. The understanding established here on the excitation of a single SW mode gives a useful guide how to tailor both magnetic layer and phonon pulse such that SWs of particular frequencies are excited.

ACKNOWLEDGMENTS

The work was supported by the Deutsche Forschungsgemeinschaft (BA 1549/14-1), the European Community's Seventh Framework Programme under Grant Agreement No. 214954 (HERODOT), the Russian Foundation for Basic Research, the Russian Academy of Sciences, and the National Science Foundation Grant DMR10-05851.

APPENDIX: THEORY OF SPIN WAVE EXCITATION BY STRAIN PULSES

In order to describe in detail the spin wave excitation process by a strain pulse, we consider the dynamics of the magnetization $\mathbf{M}$ within the macroscopic model by Landau and Lifshitz, neglecting dissipation[19] as described by Eq. (2). The Landau-Lifshitz equation is complemented by the boundary conditions through introducing the magnetic surface energy, F_{surf}, which is assumed as $F_{\text{surf}} = K_s \cos^2\theta$, where θ is the angle between the magnetization and the external normal to the surface, $\mathbf{n}$. A positive or negative value of the surface magnetic energy parameter K_s corresponds to an in-plane or normal orientation of the surface easy axis. Accordingly, the boundary conditions are $\mathbf{M} \times (D\frac{\partial \mathbf{M}}{\partial \mathbf{n}} + 2\mathbf{n}K_s \cos\theta) = 0$.[23]

Although the mathematical approach to simulation of the magnetization dynamics is quite clear, such problems are rarely solved straightforwardly. The Landau-Lifshitz equation in spectral representation is a fourth-order differential equation and the solution for the SW modes in the film involves some cumbersome algebra (see Ref. 23 and references therein). Another difficulty lies in considering the magnetization excitation process originating from an external perturbation that makes impossible to use the mode expansion formalism for the magnetization in general. However, in our case in which the strain pulse drives the magnetization during a finite time, we managed to obtain a relatively simple expression for the magnetization, which at large times does correspond to the mode expansion.

It is convenient to introduce the spherical angles ϑ and φ, which characterize the direction of $\mathbf{M}$ instead of the magnetization projections: $M_z = M\cos\vartheta$, $M_y = M\sin\vartheta\sin\varphi$, and $M_x = M\sin\vartheta\cos\varphi$. The equilibrium values of ϑ and φ, ϑ_0 and φ_0, are determined by the particular forms of F and F_{surf}. Because F contains magnetoelastic terms, the strain pulse drives the magnetization out of equilibrium, causing its precession, which persists even after the pulse has left the film. Within the linear-response model, we assume $\vartheta \approx \vartheta_0 + \delta\vartheta$ as well as $\varphi \approx \varphi_0 + \delta\varphi$, and obtain for $\delta\vartheta$ and $\delta\varphi$ the following equations:

$$\frac{\partial \delta\vartheta}{\partial t} = \frac{\gamma}{\sin\vartheta_0}\Big[-\overline{F}''_{\vartheta\varphi}\delta\vartheta - \overline{F}''_{\varphi\varphi}\delta\varphi + D\sin^2\vartheta_0 \frac{\partial^2\delta\varphi}{\partial z^2} - \overline{F}''_{\varphi\varepsilon}\varepsilon(z,t)\Big],$$

$$\frac{\partial \delta\varphi}{\partial t} = \frac{\gamma}{\sin\vartheta_0}\left[\overline{F}''_{\vartheta\vartheta}\delta\vartheta + \overline{F}''_{\vartheta\varphi}\delta\varphi - D\frac{\partial^2\delta\vartheta}{\partial z^2} - \overline{F}''_{\vartheta\varepsilon}\varepsilon(z,t)\right]. \tag{A1}$$

Here, $\overline{F} \equiv F/M_0$ and the derivatives are taken at the equilibrium values ϑ_0 and φ_0. The boundary conditions for Eq. (A1)

are

$$\frac{\partial \delta\vartheta}{\partial z} = \pm\frac{1}{l^*}\delta\vartheta, \quad \frac{\partial \delta\varphi}{\partial z} = 0, \tag{A2}$$

where $l^* = M_0 D/(2K_s)$ and the + and − signs correspond to $z = 0$ and d, respectively. We do not analyze here the explicit form of the free energy and the equilibrium directions of the magnetization, which was done in detail in Ref. 12. It is important that if the easy axes for the bulk and the surface are not parallel to each other, the steady-state magnetization in the film can be, in general, spatially nonuniform, and the coefficients in Eq. (A1) become z dependent. Below we assume that this is not the case. We will also show that for the magnetic boundary conditions that allow selective excitation of spin wave modes, the equilibrium magnetization is in fact uniform.

It is convenient to perform a Fourier transformation of Eq. (A1). This results in fourth-order differential equations in the variable$z$. We therefore obtain four wave vectors q for a given frequencyω:

$$q^2 = \frac{1}{\gamma^2 D^2}\left[-v_m^2 \pm \sqrt{v_m^4 + \gamma^2 D^2(\omega^2 - \omega_u^2)}\right], \tag{A3}$$

where $\omega_u = \gamma\sqrt{\overline{F}''_{\vartheta\vartheta}\overline{F}''_{\varphi\varphi} - (\overline{F}''_{\vartheta\varphi})^2}(\sin\vartheta_0)^{-1}$ is the frequency of the spatially uniform magnetization precession and $v_m^2 = \gamma^2 D(\overline{F}''_{\varphi\varphi}/\sin^2\vartheta_0 + \overline{F}''_{\vartheta\vartheta})/2$. In a bulk, ferromagnetic crystal v_m determines the dispersion of spin waves. In particular, for ω close to ω_0, we have $\omega \approx \omega_0 + v_m^2 q^2/\omega_0$. Once these wave vectors are known, it is straightforward to calculate the solution of the spectral analog of Eq. (A1) using the variation-of-parameters method. The resulting constants are determined by the boundary conditions (A2) by which the solutions for the spectral components $\delta\varphi_\omega(z)$ and $\delta\vartheta_\omega(z)$ become uniquely fixed. Then, the temporal evolution of the magnetization can be obtained through the inverse Fourier transform. The form of the solutions $\delta\varphi_\omega(z)$ and $\delta\vartheta_\omega(z)$ allows one to perform the analysis of the magnetization dynamics for times when the strain pulse has left the film. $\delta\varphi_\omega(z)$ and $\delta\vartheta_\omega(z)$ can be split into resonant and transient parts: $\delta\varphi_\omega(z) = \delta\varphi_\omega^{(\mathrm{res})}(z) + \delta\varphi_\omega^{(\mathrm{tr})}(z)$ and $\delta\vartheta_\omega(z) = \delta\vartheta_\omega^{(\mathrm{res})}(z) + \delta\vartheta_\omega^{(\mathrm{tr})}(z)$. For the resonant part, we have

$$\begin{aligned}
\delta\vartheta_\omega^{(\mathrm{res})}(z) &= \frac{1}{\Delta_e(\omega)}\vartheta_e(z)\int_0^d dz\varepsilon_\omega(z)[\varsigma_\vartheta\vartheta_e(z) + \varsigma_\varphi\varphi_e(z)] \\
&\quad + \frac{1}{\Delta_o(\omega)}\vartheta_o(z)\int_0^d dz\varepsilon_\omega(z)[\varsigma_\vartheta\vartheta_o(z) + \varsigma_\varphi\varphi_o(z)], \\
\delta\varphi_\omega^{(\mathrm{res})}(z) &= \frac{1}{\Delta_e(\omega)}\varphi_e(z)\int_0^d dz\varepsilon_\omega(z)[\varsigma_\vartheta\vartheta_e(z) + \varsigma_\varphi\varphi_e(z)] \\
&\quad + \frac{1}{\Delta_o(\omega)}\varphi_o(z)\int_0^d dz\varepsilon_\omega(z)[\varsigma_\vartheta\vartheta_o(z) + \varsigma_\varphi\varphi_o(z)].
\end{aligned} \tag{A4}$$

In this equation, the zeroes of Δ_e and Δ_o correspond to the eigenfrequencies of even and odd free spin wave (SW) modes of the film, and $\vartheta_{e,o}$, $\varphi_{e,o}$ are the corresponding eigenmodes. The explicit expressions for $\Delta_{e,o}$ and $\vartheta_{e,o}$, $\varphi_{e,o}$ are

$$\begin{aligned}
\Delta_e &= \sin\frac{q_2 d}{2}(\overline{F}''_{\vartheta\varphi} + i\omega\sin\vartheta_0/\gamma)^{-1}\left\{\overline{F}''_{\vartheta\vartheta}\left(q_1\sin\frac{q_1 d}{2}\cot\frac{q_2 d}{2} - q_2\cos\frac{q_1 d}{2}\right)\right. \\
&\quad \left. + D\left[\left(q_2^2 - q_1^2\right)q_1 q_2 l^*\sin\frac{q_1 d}{2} - q_2^3\cos\frac{q_1 d}{2} + q_1^3\sin\frac{q_1 d}{2}\cot\frac{q_2 d}{2}\right]\right\}, \\
\Delta_o &= \sin\frac{q_2 d}{2}\cot\frac{q_1 d}{2}(\overline{F}''_{\vartheta\varphi} + i\omega\sin\vartheta_0/\gamma)^{-1}\left\{\overline{F}''_{\vartheta\vartheta}\left(q_2\sin\frac{q_1 d}{2} - q_1\cos\frac{q_1 d}{2}\tan\frac{q_2 d}{2}\right)\right. \\
&\quad \left. + D\left[\left(q_2^2 - q_1^2\right)q_1 q_2 l^*\cos\frac{q_1 d}{2} + q_2^3\sin\frac{q_1 d}{2} - q_1^3\cos\frac{q_1 d}{2}\tan\frac{q_2 d}{2}\right]\right\}, \\
\vartheta_e &= \cos q_1(z - d/2) - \frac{\left(\overline{F}''_{\vartheta\vartheta} + Dq_1^2\right)q_1\sin\frac{q_1 d}{2}}{\left(\overline{F}''_{\vartheta\vartheta} + Dq_2^2\right)q_2\sin\frac{q_2 d}{2}}\cos q_2(z - d/2), \\
\varphi_e &= \xi_1\left[\cos q_1(z - d/2) - \frac{q_1\sin\frac{q_1 d}{2}}{q_2\sin\frac{q_2 d}{2}}\cos q_2(z - d/2)\right], \\
\vartheta_o &= \sin q_1(z - d/2) - \frac{\left(\overline{F}''_{\vartheta\vartheta} + Dq_1^2\right)q_1\cos\frac{q_1 d}{2}}{\left(\overline{F}''_{\vartheta\vartheta} + Dq_2^2\right)q_2\cos\frac{q_2 d}{2}}\sin q_2(z - d/2), \\
\varphi_o &= \xi_1\left[\sin q_1(z - d/2) - \frac{q_1\cos\frac{q_1 d}{2}}{q_2\cos\frac{q_2 d}{2}}\sin q_2(z - d/2)\right],
\end{aligned} \tag{A5}$$

where the q_1^2 and q_2^2 correspond to the plus or the minus signs in Eq. (4) and $\xi_{1,2} = -(\overline{F}''_{\vartheta\vartheta} + Dq_{1,2}^2)(\overline{F}''_{\vartheta\varphi} + i\omega \sin\vartheta_0/\gamma)^{-1}$. The coefficients $\varsigma_{\vartheta,\varphi}$ are given by

$$\varsigma_\vartheta = \frac{q_2 \sin\frac{q_2 d}{2}}{q_1 \sin\frac{q_1 d}{2}} \frac{\overline{F}''_{\vartheta\varepsilon}\xi_2^2}{2(\xi_1 - \xi_2)D},$$
$$\varsigma_\varphi = \frac{q_2 \sin\frac{q_2 d}{2}}{q_1 \sin\frac{q_1 d}{2}} \frac{\overline{F}''_{\varphi\varepsilon}\xi_2}{2\xi_1(\xi_1 - \xi_2)D \sin^2\vartheta_0}. \quad \text{(A6)}$$

The resonant Fourier components have poles at the frequencies of the SW modes. This allows us to perform the inverse Fourier transformation for them analytically, which provides harmonic time dependencies for $\delta\vartheta^{(\mathrm{res})}(z,t)$ and $\delta\varphi^{(\mathrm{res})}(z,t)$:

$$\delta\vartheta^{(\mathrm{res})}(z,t) = \sum_n C^{(n)}\vartheta^{(n)}(z)\cos\left(\omega_n t + \alpha_\vartheta^{(n)}\right),$$
$$\delta\varphi^{(\mathrm{res})}(z,t) = \sum_n C^{(n)}\varphi^{(n)}(z)\cos\left(\omega_n t + \alpha_\varphi^{(n)}\right). \quad \text{(A7)}$$

Here, the summation goes over the spin wave eigenmodes and the index n gives both the mode number and parity with n being even or odd for spatially even and odd modes, respectively. $C^{(n)}$, $\alpha_\vartheta^{(n)}$, and $\alpha_\varphi^{(n)}$ are amplitude and phases for the mode n. Note that Eq. (8) accounts explicitly for different oscillation phases of $\delta\vartheta^{(\mathrm{res})}(z,t)$ and $\delta\varphi^{(\mathrm{res})}(z,t)$, and the eigenfunctions $\vartheta^{(n)}(z)$ and $\varphi^{(n)}(z)$ of Eq. (A7) must be modified accordingly from those of Eq. (A5). Specifically, in the expressions for $\varphi_{e,o}(z)$ in Eq. (A5), one has to take the factor $|\xi_1|$ instead of ξ_1. In the paper, we define the eigenmodes in terms of the magnetization projections rather than angles ϑ and φ. Of course, both formulations are equivalent. While operation with ϑ and φ is the adequate choice in the used mathematical routine, reformulation of the final results in terms of magnetization projections is convenient because of the used optical method of precession detection. In the actual geometry, where the equilibrium magnetization is close to the [100] direction, the projections of the eigenmodes are $S_x^{(n)}(z) = 0$, $S_y^{(n)}(z) = \varphi^{(n)}(z)$, and $S_z^{(n)}(z) = -\vartheta^{(n)}(z)$. The expression for the mode amplitudes $C^{(n)}$ can be easily obtained from Eq. (A4). We are not aiming to obtain a quantitative expression, but note that they are proportional to the overlap integrals $\int_0^d dz\varepsilon^{(n)}(z)\vartheta_n(z)$ and $\int_0^d dz\varepsilon^{(n)}(z)\varphi_n(z)$, where $\varepsilon^{(n)}(z)$ is the Fourier component of the strain corresponding to the frequency of the nth spin wave mode. Now let us return to the analysis of the spectrum of the SW modes. In fact, we are interested in the modes with frequencies close to ω_0. In this case, we have the following approximate expressions for the wave vectors q_1 and q_2:

$$q_1 = \frac{\sqrt{(\omega^2 - \omega_u^2)/2}}{v_m}, \quad q_2 = i\kappa_2, \quad \kappa_2 = \frac{\sqrt{2}v_m}{\gamma D}. \quad \text{(A8)}$$

For typical material parameters, κ_2 is a few tenths of inverse nanometers, while q_1, as we will see below, is of the order of $1/d$. From this estimate, it follows that the SW mode structure is determined mainly by the terms proportional to $\cos q_1(z - d/2)$ or $\sin q_1(z - d/2)$ for even or odd modes, respectively, while the $\cosh\kappa_2(z - d/2)$ or $\sinh\kappa_2(z - d/2)$ contributions perturb the magnetization only slightly in the thin regions very close to the interfaces. Hence in the following analysis we will neglect these latter contributions.

Since κ_2 is almost independent on frequency, the dispersion relations set to zero for even and odd SW modes, $\Delta_e = 0$ and $\Delta_o = 0$, respectively, can be considered as equations for finding q_1. Taking into account that $q_1 \ll \kappa_2$ and $\kappa_2 d \gg 1$, we get in this approximation the dispersion relations:

$$\frac{q_1 d}{2}\tan\frac{q_1 d}{2} = R \quad \text{(A9)}$$

for even modes and

$$\frac{q_1 d}{2}\cot\frac{q_1 d}{2} = -R \quad \text{(A10)}$$

for odd modes, where

$$R = \frac{\kappa_2 d}{2}\frac{\overline{F}''_{\varphi\varphi}/\sin^2\vartheta_0}{\overline{F}''_{\vartheta\vartheta} + (\overline{F}''_{\vartheta\vartheta} + \overline{F}''_{\varphi\varphi}/\sin^2\vartheta_0)\kappa_2 l^*}. \quad \text{(A11)}$$

Naturally, for different material and surface parameters, one gets a broad variety of SW spectra and eigenmodes. Apparently, the solution of the dispersion equations (A9) and (A10) corresponds to effective pinning, if $|R| \gg 1$. However, for large negative R in addition to SW modes with real q_1, two surface-like modes with imaginary q_1 appear.

[1] A. Kirilyuk, A. V. Kimel, and T. Rasing, Rev. Mod. Phys. **82**, 2731 (2010), and references therein.

[2] H. Kurebayashi, O. Dzyapko, V. E. Demidov, D. Fang, A. J. Ferguson, and S. O. Demokritov, Nat. Mater. **10**, 660 (2011).

[3] S. T. B. Goennenwein, T. Graf, T. Wassner, M. S. Brandt, M. Stutzmann, J. B. Philipp, R. Gross, M. Krieger, K. Zürn, P. Ziemann, A. Koeder, S. Frank, W. Schoch, and A. Waag, Appl. Phys. Lett. **82**, 730 (2003).

[4] T. G. Rappoport, P. Redlinski, X. Liu, G. Zaránd, J. K. Furdyna, and B. Jankó, Phys. Rev. B **69**, 125213 (2004).

[5] D. M. Wang, Y. H. Ren, X. Liu, J. K. Furdyna, M. Grimsditch, and R. Merlin, Phys. Rev. B **75**, 233308 (2007).

[6] X. Liu, Y. Y. Zhou, and J. K. Furdyna, Phys. Rev. B **75**, 195220 (2007).

[7] M. Sperl, A. Singh, U. Wurstbauer, S. K. Das, A. Sharma, M. Hirmer, W. Nolting, C. H. Back, W. Wegscheider, and G. Bayreuther, Phys. Rev. B **77**, 125212 (2008).

[8] C. Bihler, W. Schoch, W. Limmer, S. T. B. Goennenwein, and M. S. Brandt, Phys. Rev. B **79**, 045205 (2009).

[9] C. Thomsen, H. T. Grahn, H. J. Maris, and J. Tauc, Phys. Rev. B **34**, 4129 (1986).

[10] H.-Y. Hao and H. J. Maris, Phys. Rev. B **63**, 224301 (2001).

[11] A. V. Scherbakov, A. S. Salasyuk, A. V. Akimov, X. Liu, M. Bombeck, C. Bruggemann, D. R. Yakovlev, V. F. Sapega, J. K. Furdyna, and M. Bayer, Phys. Rev. Lett. **105**, 117204 (2010).

[12] T. L. Linnik, A. V. Scherbakov, D. R. Yakovlev, X. Liu, J. K. Furdyna, and M. Bayer, Phys. Rev. B **84**, 214432 (2011).

[13]L. Thevenard, E. Peronne, C. Gourdon, C. Testelin, M. Cubukcu, E. Charron, S. Vincent, A. Lemaître, and B. Perrin, Phys. Rev. B **82**, 104422 (2010).

[14]B. Beschoten, P. A. Crowell, I. Malajovich, D. D. Awschalom, F. Matsukura, A. Shen, and H. Ohno, Phys. Rev. Lett. **83**, 3073 (1999).

[15]A. V. Kimel, G. V. Astakhov, A. Kirilyuk, G. M. Schott, G. Karczewski, W. Ossau, G. Schmidt, L. W. Molenkamp, and Th. Rasing, Phys. Rev. Lett. **94**, 227203 (2005).

[16]The calculations were carried out in the frame of the theoretical model described in detail in Ref. 12. The best agreement with the experimental data was obtained for the following parameters of magnetocrystalline anisotropy: perpendicular uniaxial field $B_{2\perp} =$ 48 mT, in-plane uniaxial field $B_{2\parallel} = 15$ mT, perpendicular cubic field $B_{4\perp} = -33$ mT, and in-plane cubic field $B_{4\parallel} = -36$ mT.

[17]J. W. Tucker and V.W. Rampton, *Microwave Ultrasonics in Solid State Physics* (North-Holland, Amsterdam, 1972).

[18]M. Pomerantz, Phys. Rev. Lett. **7**, 312 (1961).

[19]E. M. Lifshits and L. P. Pitaevskii, *Statistical Physics* (Pergamon, Oxford, 1980), Vol. 2.

[20]L. Dreher, D. Donhauser, J. Daeubler, M. Glunk, C. Rapp, W. Schoch, R. Sauer, W. Limmer, Phys. Rev. B **81**, 245202 (2010).

[21]G. Tas and H. J. Maris, Phys. Rev. B **49**, 15046 (1994).

[22]P. J. S. van Capel and J. I. Dijkhuis, Phys. Rev. B **81**, 144106 (2010).

[23]A. G. Gurevich, G. A. Melkov, *Magnetization Oscillations and Waves* (CRC-Press, Boca Raton, 1996).

[24]C. Kittel, Phys. Rev **110**, 1295 (1958).

[25]M. F. Pascual Winter, G. Rozas, A. Fainstein, B. Jusserand, B. Perrin, A. Huynh, P. O. Vaccaro, and S. Saravanan, Phys. Rev. Lett. **98**, 265501 (2007).

[26]R. P. Beardsley, A. V. Akimov, M. Henini, and A. J. Kent, Phys. Rev. Lett. **104**, 085501 (2010).

[27]P. M. Walker, A. J. Kent, M. Henini, B. A. Glavin, V. A. Kochelap, and T. L. Linnik, Phys. Rev. B **79**, 245313 (2009).